Colloid Polym Sci (2003) 281: 951–956
DOI 10.1007/s00396-002-0858-x

ORIGINAL CONTRIBUTION

Shaofeng Wang
Yuan Hu
Zhenlong Li
Zhengzhou Wang
Yonglong Zhuang
Zuyao Chen
Weicheng Fan

Flammability and phase-transition studies of nylon 6/montmorillonite nanocomposites

Received: 24 September 2002
Accepted: 10 December 2002
Published online: 5 March 2003

S. Wang · Y. Hu (✉) · Z. Wang · W. Fan
State Key Laboratory of Fire Science, University of Science and Technology of China, 230029 Hefei, Anhui, China
E-mail: yuanhu@ustc.edu.cn
Tel.: +86-551-3601664
Fax: +86-551-3601664

S. Wang · Z. Li · Z. Chen
Department of Chemistry, University of Science and Technology of China, 230026 Hefei, Anhui, China

Y. Zhuang
Structure Research Laboratory, Anhui University, 230026 Hefei, Anhui, China

Abstract Nylon 6 (PA6)/clay hybrids have been prepared using a direct melt intercalation technique by two processes. One is PA6 melt-mixing with modified clay, the other is PA6 melt-mixing with natural (Na^+ base) clay using an ammonium salt bearing long alkyl chains as a polymer/clay reactive compatibilizer. Their structure and flammability properties are characterized by X-ray diffraction, transmission electron microscopy and cone calorimeter experiments. The results of the cone calorimeter experiments show that hybrids made by these two processes have a lower heat release rate peak and higher thermal stability than that of original PA6. Meanwhile, X-ray diffraction was used to investigate PA6/clay hybrids with various cooling histories from the melt, including medium-rate cooling (air cooling) and rapid cooling (water-quenched). In contrast to pure PA6 dominated by the α phase, the addition of clay silicate layers by these two methods favors the formation of the γ crystalline phase in PA6/clay hybrids. Flammability and phase-transition studies confirm that silicate layers added by these two methods have a similar nanoeffect and nanodispersion in the PA6 matrix.

Keywords Nylon 6 · Nanocomposites · X-ray diffraction · Crystallization

Introduction

Recently, much attention has been paid to polymer nanocomposites, especially polymer-layered silicate nanocomposites, which represent a rational alternative to conventional filled polymers. Nanocomposite technology has been described as the next great frontier of material science. By employing minimal addition levels (below 10 wt%), nanoclays enhance mechanical, thermal, dimensional and barrier performance properties significantly [1, 2, 3].

The most commonly used clay is the smectite group mineral, such as montmorillonite (MMT), which is a naturally occurring 2:1 phyllosilicate. The structure consists of two fused silica tetrahedral sheets sandwiching an edge-shared octahedral sheet of either aluminium or magnesium hydroxide. In pristine form the excess negative charge is balanced by cations (Na^+, Li^+, Ca^{2+}), which exist hydrated in the interlayer. Obviously, in this pristine state MMT is immiscible with hydrophobic polymer. Traditionally, in order to facilitate silicate layer interaction with a polymer, the clay is modified with an alkylammonium salt (surfactant molecule) by a cation-exchange reaction, because the alkylammonium makes the hydrophilic clay surface organophilic.

Nylon 6 (PA6) is an important engineering resin, widely used in fibre, film and engineering thermoplastic, where the properties of thermal stability and fire resistance are priorities. The first polyamide/clay

nanocomposites were reported as early as 1976 by Fujiwara and Sakomoto [4]. One decade later, a research team from Toyota disclosed improved methods for producing PA6/clay nanocomposites using an in situ polymerization method, by which very moderate inorganic loadings resulted in concurrent and remarkable enhancements of thermal and mechanical properties [5, 6]. In the same year, Vaia et al. [7] found that it is possible to melt-mix polymers with clays without the use of organic solvents. Since then, the nanocomposites have become more widely studied in academic, government and industrial laboratories. The technique of melt processing is particularly attractive owing to its versatility and compatibility with existing processing infrastructure and is beginning to be used for commercial applications [8, 9]. However, the technique of melt processing uses premodified clay as a raw material, which will produce waste water and increase cost. Recently, Alexandre et al. [10] reported a novel technique for the preparation of ethylene vinyl acetate/clay nanocomposites starting directly from natural (Na^+ base) clay using an ammonium salt bearing long alkyl chains as a polymer/clay reactive compatibilizer. Synthesis of polymer/clay nanocomposites through direct melting with inorganic MMT using an ammonium salt bearing long alkyl chains as a reactive compatibilizer is a new method. This method is a more efficient and environmentally benign alternative than other methods and would greatly expand the practical applications of these materials.

In the present work, we synthesized PA6/MMT nanocomposites (PA6CNs) through a direct melt intercalation technique by two processes: one is PA6 melting with modified MMT; the other is PA6 melting with natural (Na^+ base) MMT using an ammonium salt bearing long alkyl chains as a reactive compatibilizer. The morphology, crystalline phase transition and fire properties of the two PA6CNs were studied by X-ray diffraction (XRD), transmission electron microscopy (TEM) and cone calorimeter experiments. This paper is the first report of the characterization of PA6CNs made by PA6 melt-mixing with natural (Na^+ base) clay using an ammonium salt bearing long alkyl chains as a polymer/clay reactive compatibilizer.

Experimental

Materials

PA6(1003NW8, with weight-average molecular weight 18,000) was supplied as pellets by UBE Industries, Japan. The original purified sodium MMT, (with a cation-exchange capacity of 96 mEq/100 g and interlayer spacing $d_{001} = 14.5$ Å) and organophilic montmorillonite (OMT, with interlayer spacing $d_{001} = 24$ Å) were kindly provided by Keyan Company, Hefei, China. OMT was prepared from MMT by an ion-exchange reaction using hexadecyltrimethylammonium bromide (C16) in water according to the reported method [1]. The MMT and OMT used in this study were ground and passed through a 400 mesh.

The preparatlion of PA6/clay hybrid

1. Process 1: PA6 granules were dried in a vacuum oven at 110 °C for 10 h and then melt-mixed with 5 wt% OMT at 245 °C using a twin-screw mill (XK-160, made in Jiangshu, China) for 10 min to yield a hybrid, termed PA6/OMT.
2. Process 2: PA6 granules were melt-mixed with 5 wt% MMT and 3 wt % C16 under the same condition as in process 1, and the hybrid was termed PA6/MMT/C16.

Evaluation of dispersibility of the clay in PA6 resin matrix

The dispersibility of the silicate layers in the PA6 was evaluated using XRD, bright-field TEM. The thin films (1 mm) of the hybrids were pressed at 245 °C for the XRD measurements to evaluate the dispersibilities of the silicate layers in the PA6 matrix. The XRD experiments were performed at room temperature using a Japan Rigaku D/max-rA X-ray diffractionmeter (30 kV, 10 mA) with Cu ($\lambda = 1.54178$ Å) irradiation at a rate of 2°/min in the range 1.5–10°. TEM specimens were cut from an epoxy block with the embedded PA6 hybrid powders at room temperature using an ultramicrotome (Ultracut-1, UK) with a diamond knife. Thin specimens, 50–80 nm, were collected in a trough filled with water and placed on 200 mesh copper grids. TEM images were obtained using a JEOL JEM-100SX with an acceleration voltage of 100 kV.

Cone calorimetry

Samples (100×100×3 mm^3) were exposed to a Stanton Redcroft cone calorimeter at an incident heat of 50 kW/m^2 according to ASTM 1356-90. The peak heat release rate (HRR), mass loss rate, specific extinction area, ignition time, and specific heat of combustion data were reproducible to within 10% when measured at 50 kW/m^2. The cone data reported here are the averages of three replicated experiments.

Phase-transition analyses

The $\gamma \rightarrow \alpha$ crystalline phase transition in PA6/clay hybrids with various cooling histories from the melt, including medium-rate cooling (air cooling) and rapid cooling (water-quenched), were investigated by XRD. Films (1 mm) of the hybrids were prepared as follows. The hybrids were pressed at 245 °C using a flat-sulfureted machine (HPC-100,China) for the XRD measurements. Two kinds of cooling conditions were then used.

1. Medium-rate cooling: the films were kept on the 245 °C flat-sulfureted machine for 10 min and then removed and cooled in air at room temperature.
2. Rapid cooling: the films were kept on the 245 °C flat-sulfureted machine for 10 min and then removed and quenched in a water bath at room temperature.

XRD experiments were performed at room temperature using a Japan Rigaku D/max-rA X-ray diffractionmeter (30 kV, 10 mA) with Cu ($\lambda = 1.54178$ Å) irradiation at a rate of 2°/min in the range 10–30°.

Result and discussion

Dispersibility of PA6/clay hybrids

We assume that the cooling rate or crystallization process does not drastically alter the mean distribution of the silicate. The XRD patterns of the MMT,OMT, PA6/MMT hybrid, with MMT mass fraction 5 wt%, PA6/OMT hybrid, with OMT mass fraction 5 wt%, and PA6/MMT/C16 hybrid, with MMT mass fraction 5 wt% and C16 mass fraction 3 wt%, are shown in Fig. 1. The peaks correspond to the (001) plane reflections of the clays. Both PA6/OMT and PA6/MMT/C16 have broadened d_{001} peaks and visible d_{002} peaks. PA6/OMT has a 0.8-nm gallery height increase compared to that of OMT and PA6/MMT/C16 has a 1.4-nm gallery height increase compared to that of OMT, which indicates an intercalated–delaminated structure (Fig. 1traces d, e). The different d_{001} peaks between PA6/OMT and PA6/MMT/C16 may be due to the different mechanism of intercalation. However, it is difficult from XRD to draw definitive conclusions about the defined structure. Thus, TEM techniques are necessary to characterize the morphology of the nanocomposites. The black lines correspond to clay layers. The TEM photographs (Figs. 2, 3) for PA6/OMT and PA6/MMT/C16 display a good dispersion of the clay layers, and both intercalated (stacks of multilayers of clay) and delaminated structures coexist, although isolated particles are observed to a lesser extent in PA6/MMT/C16 compared to the nanocomposite directly obtained with OMT (PA6/OMT).

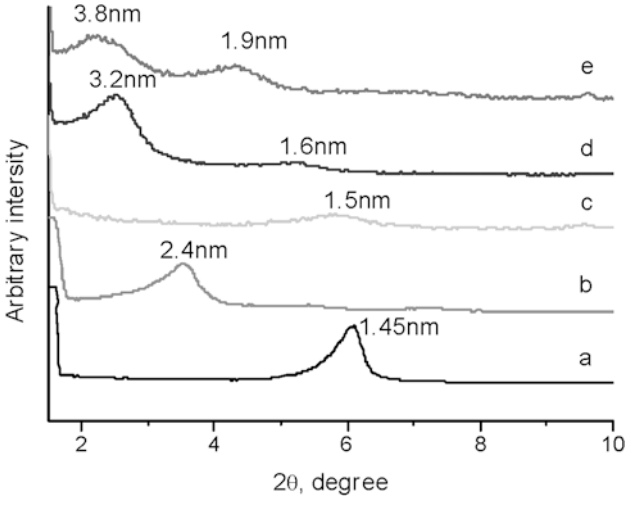

Fig. 1 X-ray diffraction (*XRD*) patterns of *a* sodium montmorillonite (*MMT*), *b* organophilic montmorillonite (*OMT*), *c* nylon 6 (*PA6*)/MMT hybrid, with MMT mass fraction 5 wt%, *d* PA6/OMT hybrid, with OMT mass fraction 5 wt%, and *e* PA6/MMT/hexadecyltrimethylammonium bromide (*C16*) hybrid, with MMT mass fraction 5 wt% and C16 mass fraction 3 wt%

To compare the effect of the nanodispersion of the silicate, a microcomposite (PA6/MMT) was prepared by melt-mixing PA6 with MMT. The XRD for PA6/MMT exhibits only a weak peak corresponding to an interlayer distance of 1.5 nm, assimilated to the interlayer distance of nonmodified MMT (Fig.1traces a, c). The primary particles composed of many silicate layers can be seen in the TEM image of PA6/MMT (black one in Fig. 4). This situation corresponds to that of a conventional filled polymer where primary particles measuring a few microns are dispersed in the matrix.

Flammability properties of PA6/clay hybrids

Characterization of the flammability properties of a variety of polymer/clay nanocomposites, under firelike conditions, using the cone calorimeter has revealed improved flammability properties for many types of

Fig. 2 Transmission electron microscope (*TEM*) image of a nanocomposite based on PA6 filled with 5 wt% OMT (PA6/OMT)

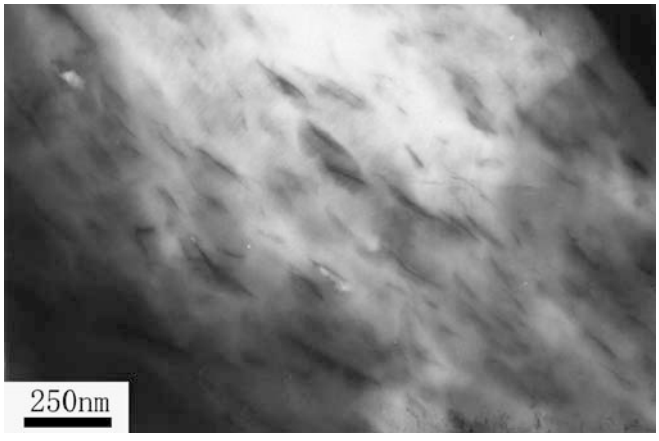

Fig. 3 TEM image of a nanocomposite based on PA6 filled with 5 wt% MMT and 3 wt% C16 (PA6/MMT/C16)

Fig. 4 TEM image of a microcomposite based on PA6 filled with 5 wt% MMT (PA6/MMT)

polymer/clay nanocomposites [11, 12, 13, 14, 15]. The cone calorimeter is one of the most effective bench-scale methods for studying the flammability properties of materials. The HRR, in particular the peak HRR, has been found to be the most important parameter to evaluate fire safety [11].

The HRR plots for pure PA6, PA6/MMT microcomposite, PA6/OMT and PA6/MMT/C16 nanocomposies at 50 kW/m^2 are shown in Fig. 5. The peak HRR of PA6/MMT is 16% lower than that of pure PA6. Its peak HRR is lower partly because it contains 95 wt% PA6. However, the peak HRRs of PA6/OMT and PA6/MMT/C16 nanocomposites are 40%, 32% lower than that of pure PA6, respectively.

Studies [11, 12, 13, 14, 15, 16, 17] have shown that the lower flammability of polymer/clay nanocomposites is not due to retention of a large fraction of fuel, but in the form of carbonaceous char, in the condensed phase. The nanodispersed lamellae of clay (exfoliation or intercalation) in the polymer matrix all enhance the formation of char when burning. After pyrolysis, the nanocomposite forms char with a multilayered carbonaceous-silicate structure. This high-performance carbonaceous silicate char builds up on the surface during burning; this insulates the underlying material and slows the escape of the volatile products generated during decomposition.

The variation in the HRR peak decrease may be explained by the difference in structure observed between the two nanocomposites (PA6/OMT and PA6/MMT/C16). The silicate layers in PA6/OMT disperse more uniformly than in PA6/MMT/C16 (Figs. 2, 3). These better nanodisperse silicate layers correspond to better high-performance carbonaceous silicate char on the surface when burning and a lower HRR peak in PA6 matrix.

Effect of structure on the phase transition of PA6/clay hybrids

The main phases of PA6 are the α phase and the γ phase. The crystalline structure of PA6 under equilibrium conditions and at room temperature is the α phase and PA6 is most stable in the α phase. The γ phase is metastable and it can be transformed into the α phase by annealing. However, the γ phase becomes the dominant phase in the PA6/clay nanocomposites [18, 19, 20]. The reason why the silicate layers favors the formation of the γ phase in PA6 still remains unclear and it may be related to the interaction between clay layers and PA6 molecules. Lincoln et al. [19] suggested that the addition of clay layers forces the amide groups of PA6 out of the plane formed by the chains. This results in conformational changes of the chains, which limits the formation

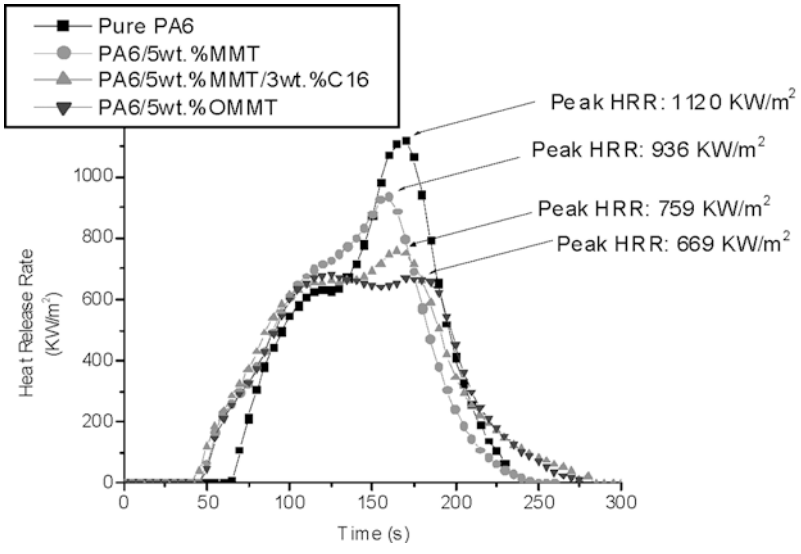

Fig. 5 Heat release rate (*HRR*) data for pure PA6, PA6/MMT, PA6/OMT and PA6/MMT/C16 hybrids

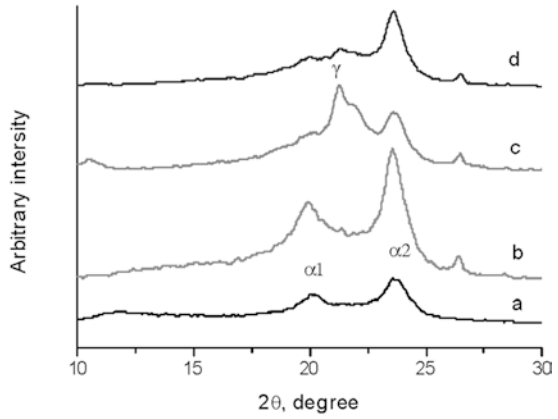

Fig. 6 XRD patterns of *a* pure PA6, *b* PA6/MMT, *c* PA6/OMT and *d* PA6/MMT/C16, under the medium-rate cooling (air cooling) condition

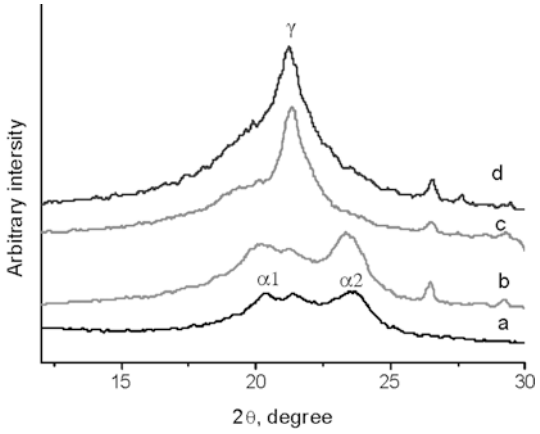

Fig. 7 XRD patterns of *a* pure PA6, *b* PA6/MMT, *c* PA6/OMT and *d* PA6/MMT/C16, under the rapid cooling (water-quenched) condition

of hydrogen-bonded sheets and the γ phase is favored. According to this assumption, the structure of the silicate layers dispersed in PA6/clay hybrids will greatly affect the phase structure of the PA6 matrix.

To understand how the structure of PA6/clay hybrids influences the $\gamma \rightarrow \alpha$ crystalline phase transition in the PA6 matrix with various cooling histories from the melt, including rapid cooling (water-quenched), medium-rate cooling (air cooling), we examined two kinds of PA6/clay nanocomposites (PA6/OMT and PA6/MMT/C16) by two processes compared to that of pure PA6 and PA6/MMT microcomposite. These layered silicates disperse differently in the PA6 matrix. The TEM images (Figs. 2, 3) of PA6/OMT and PA6/MMT/C16 show that they both contain intercalated MMT and delaminated MMT layers, however, the silicate layers in PA6/OMT disperse more uniformly than in PA6/MMT/C16.

The crystalline form and degree of crystallinity were determined by XRD. The effect of structure is apparent in the XRD. For the medium-rate cooling condition (Fig. 6), in pure PA6 and PA6/MMT microcomposite, both $\alpha 1$ and $\alpha 2$ peaks are very distinct and the γ peak is almost absent; however, in PA6/OMT and PA6/MMT/C16 nanocomposites, the γ peak is visible and the γ peak in PA6/OMT is more prominent than that of PA6/MMT/C16 (this may due to the better dispersed silicate layers in PA6/OMT). The $\alpha 1$ and $\alpha 2$ peaks all decrease. These results indicate that madium-rate cooling favors the formation of the α phase in pure PA6, and the nanodispersed silicate layers increase the crystallization of the γ phase, while microdispersed silicate layers have little effect on the crystalline properties of the PA6 matrix.

For the rapid cooling (water-quenched) condition (Fig. 7), in pure PA6 and PA6/MMT microcomposite, both $\alpha 1$ and $\alpha 2$ peaks are very distinct. The γ peak is weak and visible; however, in PA6/OMT and PA6/MMT/C16 nanocomposites, the γ peak is dominant with weak shoulders of $\alpha 1$ and $\alpha 2$ peaks. These results indicate that rapid cooling favors the formation of the γ phase. The addition of nanodispersed silicate layers increases the crystallization of the γ phase, while this effect cannot be found in the PA6/MMT microcomposite. This result confirms that the dispersed structure of silicate layers greatly affects the crystalline properties of the PA6 matrix. The nanodispersed silicate layers may interact with PA6 molecules and limit the formation of hydrogen-bonded sheets, and this favors the formation of the γ phase.

Conclusion

We prepared a PA6/MMT/C16 nanocomposite by PA6 melt-mixing with natural (Na^+ base) clay while using C16 as a polymer/clay reactive compatibilizer. The flammability and phase structure of PA6/MMT/C16 at different cooling conditions has been studied compared to that of the PA6/OMT nanocomposite, the PA6/MMT microcomposite and pure PA6. The results show that the dispersibility of clay layers in the PA6 matrix will greatly affect the phase transition of PA6 and the process of making the PA6 nanocomposite by PA6 melt-mixing with natural (Na^+ base) clay using C16 as a polymer/clay reactive compatibilizer is a reasonable way.

Acknowledgements The work was financially supported by the National Natural Science Foundation of China (no. 50003008), the China NKBRSF project (no. 2001CB409600), Anhui "the tenth five years" tackle key problems project and the Hefei Unit Center of Analysis and Test of CAS.

References

1. Hu Y, Song L, Xu J, Yang L, Chen Z, Fan W (2001) Colloid Polym Sci 279:819
2. Wang S. Hu Y, Song L, et al. (2002) Polym Degrad Stab 77:423
3. Alexandre M, Dubois D (2000) Mater Sci Eng 28:1
4. Fujiwara S, Sakamoto T (1976) Jpn Patent Appl 109998 (assigned to Unichika KK, Japan)
5. Okada A, Fukushima Y, Kawasumi M, Inagaki S, Usuki A, Sugiyama S, Kurauch T, Kamigaito O (1988) US Patent 4,739,007 (assigned to Toyota Motor Co., Japan)
6. Usuki A, Kojima Y, Kawasumi M, Okada A, Fukushima Y, Kurauchi T, Kamigito O (1993) J Mater Res 8:1179
7. Vaia RA, Ishii H, Giannelis EP (1993) Chem Mater 5:1694
8. Garces JM, Moll DJ, Bicerano J, Fibiger R, Mcleod DG (2000) Adv Mater 12:1835
9. Fornes TD, Yoon PJ, Hunter DL, Keskkula H, Paul DR (2002) Polymer 43:5195
10. Alexandre M, Beyer G, Henrist C, et al. (2001) Chem Mater 13:3830
11. Gilman JW (1999) Appl Clay Sci 15:31
12. Hu Y, Song L (2001) International fire safety conference (Fire Retardant Chemicals Association), 11–14 March, San Francisco
13. Bourbigot S,Le Bras M, Dabrowski F, Gilman JW, Kashiwagi T (2000) Fire Mater 24:201
14. Gilman JW, Jackson CL, Morgan AB, et al. (2000) Chem Mater 12:1866
15. Vaia RA, Price G, Ruth PN, Nguyen HT, Lichtenhan J (1999) Appl Clay Sci 15:67
16. Zanetti M, Kashiwagi T, Falqui L, Camino G (2002) Chem Mater 14:881
17. Zhu J, Morgan AB, Lamelas FJ, Wilkie CA (2001) Chem Mater 13:3174
18. Wu Q, Liu X, Berglund LA (2002) Polymer 43:2445
19. Lincoln DM, Vaia RA, Wang ZG, Hsiao BS (2001) Polymer 42:1621
20. Liu X, Wu Q (2002) Polymer 43:1933